Biosensors and Bioelectronics 295 (2026) 118256

Contents lists available at ScienceDirect

Biosensors and Bioelectronics

journal homepage: www.elsevier.com/locate/bios

Highly integrated chip for continuous chemical synthesis, purification and inline biosensoric monitoring of biological activity on stem cell-derived 3D cardiomyocyte cultures

T. Haensch [a,b,1], F.D. Zitzmann [a,1], S. Schmidt [a], C. Stanko [c], E. Paternoga [d], M. Meier [a], K. Zeitler [d], D. Belder [b], A.A. Robitzki [e], H.-G. Jahnke [a,*]

[a] Leipzig University, Institute of Biochemistry, Center for Biomedicine and Biotechnology, Deutscher Platz 5, 04103, Leipzig, Germany
[b] Leipzig University, Institute of Analytical Chemistry, Technikum Analytikum, Linnéstr. 3, 04103, Leipzig, Germany
[c] University Hospital Jena, Institute for Molecular Cell Biology, Hans-Knöll-Str. 2, 07745, Jena, Germany
[d] Leipzig University, Institute of Organic Chemistry, Johannisallee 29, 04103, Leipzig, Germany
[e] Karlsruher Institute for Technology (KIT), Hermann-von-Helmholtz-Platz 1, 76344, Eggenstein-Leopoldshafen, Germany

ARTICLE INFO

Keywords:
Electrochemical impedance spectroscopy
Selective laser etching
Free-flow electrophoresis
Drug purification
Stem cell-derived cardiomyocyte clusters

ABSTRACT

Miniaturization and development of lab-on-a-chip (LOC) devices are a fast-evolving research field. While single processes e.g. pharmacological compound testing on cells and organoids, diagnostic applications, chemical synthesis or on-chip analytics are widely developed and in use, the integration of multi-step processes such as chemical synthesis, product separation and purification in combination with biological activity monitoring of synthesis products in compact LOC devices is poorly realized. Especially the integration of label-free, biosensoric analysis techniques is still a bottleneck.

In this context, we developed an integrated microfluidic chip that combines an organic on-chip synthesis with subsequent continuous product purification and solvent-exchange by micro free flow electrophoresis (μFFE), followed by re-buffering to physiological conditions and finally, the biosensoric detection of biological activity on 3D cultures. As a proof of concept, the synthesis of the cardioactive drug propranolol from its precursor was chosen and successfully established in a continuous microfluidic setup. For sensitive detection of bioactivity, human stem cell-derived cardiomyocyte 3D cultures were used. The integration of microcavity microelectrode arrays, combined with impedance spectroscopy enabled label-free, non-invasive, real-time monitoring of propranolol isolation and purification as well as the quantification of the negative chronotropic effect of propranolol. The organoids show the typical negative chronotropic effect of propranolol in the μM range. Taken together, the entire process chain including chemical synthesis, purification, and inline monitoring of biological activity on a single LOC device, was successfully demonstrated.

1. Introduction

In recent years, there have been enormous developments in the field of chemical synthesis (Hao et al., 2019; Mende et al., 2020) in microfluidic lab-on-chip (LOC) systems. Especially organic syntheses on microfluidic chips profit from the lower amounts of starting materials, catalysts and solvents that are used, better heat and mass transfer as well as better surface area to volume ratios, significantly reduced reaction times (from days/hours down to minutes) while having product turnover rates comparable to batch syntheses (Gutmann et al., 2015), less energy consumption, and improved safety for critical process regimes (Plutschack et al., 2017; Liu et al., 2021; Capaldo et al., 2023; Hessel et al., 2024; Raby-Buck et al., 2025). Groups pursue different approaches for example the microflow synthesis of classical small molecule organic drugs (Santana et al., 2020) with yields in the range of 24 %–95 %, synthesis of bimetallic powders using a microfluidic chip as a high throughput temperature control platform (Hu et al., 2020) or the synthesis of complex materials such as carbon dots (Li et al., 2023) or

* Corresponding author.
E-mail addresses: clara.stanko@web.de (C. Stanko), kzeitler@uni-leipzig.de (K. Zeitler), belder@uni-leipzig.de (D. Belder), andrea.robitzki@kit.edu (A.A. Robitzki), heinz-georg.jahnke@bbz.uni-leipzig.de (H.-G. Jahnke).
[1] These authors contributed equally to this work.

https://doi.org/10.1016/j.bios.2025.118256
Received 11 September 2025; Received in revised form 18 November 2025; Accepted 20 November 2025
Available online 21 November 2025

biomaterials on microfluidic chips (Wang et al., 2018). State-of-the-art fabrication and integration techniques make on-chip chemical synthesis more and more interesting with regard to sustainability and green chemistry (Hessel et al., 2024) approaches as well as commercial use cases like complex pharmaceutical synthesis (Gutmann et al., 2015; Mc Veigh and Bellan, 2024; Santana et al., 2020). Furthermore, the advantage to shorten downstream work-up processes led to system integration of chemical analysis and synthesis on a chip that gave the possibility to e.g. inline feedback control loops, as well as improved product quality due to inline analysis (Gutmann et al., 2015; Hessel et al., 2024; Raby-Buck et al., 2025) and therefore, to novel integrated devices with unmatched performance in terms of speed, in-situ process control, sustainability, and economics (Das et al., 2022; Westphal et al. 2022, 2024).

In contrast, the integration of biosensoric approaches, e.g., the on-chip analysis of the bioactivity of synthesized drugs on cell cultures, is rare and severely lacking. In this context, we aim to provide a proof-of-principle demonstration that combines three distinct tasks: chemical synthesis, purification and the biosensoric detection of a reference drug, all on a *single* compact microfluidic chip. To our knowledge, this has never been achieved before. Our created MiCAPSUiD (***Mi**cro-**C**avitiy**A**rray with **P**urification and **S**ynthesis-**U**nit and **i**mpedimetric **D**etection*) system provides several important laboratory steps and might be used in point of care applications for continuous drug production.

For our demonstration, the synthesis of propranolol (Crowther and Smith, 1968), a well-known cardioactive drug with a negative chronotropic effect on cardiomyocyte cells (Nayler et al., 1969) was chosen. Although propranolol has been known as a drug for a long time and is produced in large quantities, it is still the subject of current research with regard to advantages of microflow/on-chip synthesis such as reduced synthesis time and higher yields/efficiency (Angelis et al., 2019) as well as for combinatorial synthesis/screening approaches of novel derivates (Tran et al., 2020).

Furthermore, with regard to the microfluidic/on-chip advantage for simplified integration of downstream work-up processes, the on-chip purification is a critical prerequisite for cell-based inline bioanalytic approaches to get rid of incompatible organic solvents and cytotoxic starting materials. Free-flow zone electrophoresis (Pfeiffer et al., 2018; Turgeon and Bowser, 2009) is a unique method that allows for the continuous deflection of the charged propranolol (Haensch et al., 2022), while separating the starting material and the organic solvent (Zitzmann et al., 2017b).

Additionally, one challenge when working with microfluidic chips is handling of volatile compounds. In the propranolol synthesis, usually a closed batch procedure with long reaction times (48 h, Tran et al., 2020) or high pressure (7 bar) and high temperatures (140 °C) have been used (Morodo et al., 2019) to circumvent that the volatile compound isopropylamine (bp: 32 °C–35 °C) degases or forms bubbles. An additional challenge is posed by the relatively slow ring opening of the epoxide, leading to increased reaction times when performing the reaction under standard conditions (Cepanec et al., 2003). In this paper, the fundamental concept for the MiCAPSUiD system and the subsequent optimization and functional integration of its modular steps on a compact chip is presented.

2. Materials and methods

2.1. Chip fabrication

The multi-step fabrication of the MiCAPSUiD chip, which integrates synthesis, separation/purification, and monitoring of biological activity, began with 3D glass substrate patterning using the selective laser-induced etching (SLE) process, followed by application of electrodes for free-flow electrophoresis and microcavities using the lift-off technique, as previous described (Zitzmann et al., 2022). For details, please see the method section in the supplementary information. To close the microfluidic structures, a top glass plate was bonded to the top of the microstructured glass chip plate as previously described (Jezierski et al., 2013; Zitzmann et al., 2017b), except for the microcavity area. In detail, between both plates, PEG-DA (molecular weight 258, Sigma-Aldrich, Germany) was filled with 1 % (*w/w*) 2,2-dimethoxy-2-phenylacetophenone (Sigma-Aldrich, Germany). In the mask aligner, the layout was transferred to the PEG-DA-filled chip by photopolymerization ($\lambda = 350-405$ nm; $P = 12$ mW/cm^2, illumination time 1.5 s) through a light-impermeable photomask. The residual pre-polymer was removed by low pressure and rinsing with ethanol (70 %, *v/v* in water). For final solidification of the polymer, the chip was re-exposed ($\lambda = 350-405$ nm; $P = 12$ mW/cm^2, illumination time 5 s). The hydrogel walls that separate the electrode buffer and the running buffer in the μFFE in the purification chamber were realized by polymerization of PEG-DA (molecular weight 575; with 20 % water and 1 % DMPA, Sigma-Aldrich, Germany) with an LED ($\lambda = 320$ nm; spot size 200 μm) on a movable slide. The non-polymerized monomer was removed once again.

On top of the microcavity area, a structured PDMS block for 3D culture positioning was aligned and bonded to the chip. The PDMS block was fabricated using additive 3D printing. The water-soluble polymer polyvinyl alcohol (PVA, Carl Roth, Germany) was printed in U-shape negative moulds for the positioning channels, which were placed in a Petri dish and embedded with the transparent PDMS Sylgard 184 (Dow Chemicals, USA). After 24 h of curing PDMS, the PVA was removed by placing solid PDMS structures in water at 50 °C overnight, followed by extensive rinsing with water. Finally, the PDMS structures were carefully cut to tightly fit the chip, aligning with the microcavity structures. Bonding on top of the chip was achieved by oxygen plasma treatment using a plasma generator (FEMTO A, Diener Electronics GmbH, Germany, with an oxygen partial pressure of 1.5 mbar and a power of 300 mW) for 30 s, followed by manual alignment and a post-bake step of 5 min at 65 °C. For better long-term stability, bonding edges were sealed with silicone glue (Elastosil E41, Wacker, Gremany). Silicone connection tubes were glued onto the inlets and outlets of the chip with silicon glue. Chips could be used several times when stored in water due to the hydrogel walls. All chip layouts were created in AutoCAD 2020 (Autodesk, CA, USA).

2.2. Electrochemical impedance spectroscopy measurements

For impedimetric monitoring of the human cardiomyocyte cluster (hCMC), the chips were placed in a self-developed impedance measurement board and impedance spectra were recorded with a high-precision impedance analyzer ISX-3v2 (Sciospec Scientific Instruments, Germany) and the self-developed controlling software IMA-Tadvanced in a frequency range of 500 Hz to 1 MHz (41 frequency points) and an alternating potential of ±10 mV as previously described (Fleischer et al., 2019). The cellular contribution of hCMC (relative impedance) was calculated based on recorded blank value spectra without hCMC, and the maximum relative impedance was determined using the self-developed software, IDAT (Fleischer et al., 2019). For impedimetric detection of hCMC mechanical contraction, impedance was recorded at a single frequency of 100 kHz for 15 s with 300 samples per second. Normalization, contraction peak detection, peak amplitude and peak-to-peak-interval calculation as well as determination of contraction rate, were done with the self-developed software IMA-Tadvanced. Processed data were plotted using Prism 5 (Graphpad Software Inc., USA). Statistical significance was determined by ANOVA and Sidak post-hoc test for multiple comparison and unpaired *t*-test for two group comparisons with * $p \leq 0.05$ **, $p \leq 0.01$ and ***$p \leq 0.001$.

2.3. Micro free-flow electrophoresis (μFFE)

For μFFE, the purification chamber (20 mm length) as well as all channels were rinsed with ethanol (70 %, *v/v* in water), pure water and 5 mM phosphate buffer (Carl Roth, Germany). The synthesis loop was

rinsed again with 70 % ethanol. Syringes (ILS, Germany) with volumes of 1 mL for the synthesis and 5 mL for the sheath buffer streams, as well as the electrophoresis electrode buffer streams, were used in combination with low-pressure syringe pumps (CETONI, Germany). PTFE tubes (inner diameter 750 μm, KAP 101.133, Techlab GmbH) with 1/16' fittings (XP-206, IDEX Health & Science) connected the syringes to the inlets of the chip. Flow rates were 10 μL/min for the electrophoresis electrode streams containing 1 M sodium chloride with 25 mM Triton X-100, 1 μL/min for the synthesis channel stream and 6–14 μL/min for the sheath buffer streams containing 5 mM phosphate buffer (pH 7.4).

2.4. Deep-UV laser based inline monitoring of μFFE separation

The deep-UV optical setup, as described by Haensch et al. (2022) and Hasan et al. (2022), was used to detect both propranolol and its oxirane precursor. The electrophoresis chip was placed on a microscope equipped with a motorized x-y-stage (SCAN IM, Märzhäuser Wetzlar, Germany), controlled by a TANGO 2 Desktop (Märzhäuser Wetzlar, Germany). The propranolol and oxirane signals were obtained by moving the chip with a constant velocity of 3 mm/s over the laser-detector setup. The deflection of propranolol near the outlet was evaluated by normalizing data to the hydrogel walls peaks.

2.5. Generation of human induced pluripotent stem cells derived 3D cardiomyocyte cultures

Three-dimensional cardiomyocyte cultures were generated from human induced pluripotent stem cells (hiPSC) according to Fleischer et al. (Fleischer et al., 2019). Briefly, IMR90-C04 hiPS cells (WiCell Stem Cell bank, USA) were differentiated through a precisely timed activation and inhibition of the Wnt signal pathway, resulting in contractile 2D cardiomyocyte cultures within 10–14 days. After three weeks, the contractile cardiomyocytes were dissociated and seeded in 96-well plates with V-bottom (Thermo Fisher Scientific, Nunc, Germany) with 50,000 cells in 200 μL per well. Afterwards, plates were centrifuged at 1000×*g* for 10 min. After 2–3 days, the human cardiomyocyte clusters (hCMC) were transferred to U-bottomed 96-well plates (Greiner Bio One, Germany) for long-term cultivation. About seven days after reaggregation, hCMC achieved a diameter of about 450 μm and started to contract again. For experiments, hCMC were used earliest at day 14 after reaggregation.

2.6. NMR-based analysis of product formation and yield rate

The propranolol synthesis was performed according to Crowther and Smith (1968) and Kaiser et al. (1977). Samples were dried in a concentrator (Eppendorf concentrator 5301, Hamburg, Germany) at 60 °C and reduced pressure and resolved in d^6-DMSO (Sigma-Aldrich, Germany) with 5 μmol 1,3,5-trimethoxybenzene (Fisher Scientific, MA, USA) per sample as standard. The compounds were characterized by ^{1}H NMR spectroscopy, with NMR spectra recorded on a BRUKER Avance III HD (400.13 MHz) using the d^6-DMSO solvent peaks as an internal reference for the chemical shifts. For further processing, the auto-baseline correction and auto-phase correction features of the software MestReNova (version 14.3.1) were utilized. For yield estimation, the ratio of the peaks at the chemical shift at 8.20 for the oxirane precursor and 8.25 for propranolol was calculated.

3. Results and discussion

3.1. Design and fabrication of the MiCAPSUiD system

The integration of all process chain steps, including synthesis, electrophoretic purification, buffering, and bioactive detection using 3D cultures, requires a sophisticated approach such as the MiCAPSUiD (***Mi**croCavitiy**A**rray with **P**urification and **S**ynthesis-**U**nit and **i**mpedimetric **D**etection*) system (Fig. 1A and B). In order to realize chemical synthesis with an appropriate yield, a mixing and synthesis channel with sufficient length in the cm range has to be integrated. Furthermore, glass substrates were used due to their resistance to organic solvents and high UV light transmission. Thus, all crucial elements, such as the synthesis loop, separation/purification chamber, connection channels, microcavities, and mixing structures, had to be structured within the glass substrate. To achieve this with the desired quality and resolution, selective laser etching (SLE) was employed (Fig. 1B–SI Fig. S1A). On top of the microstructured glass substrate, large platinum electrodes for coupling in the micro free-flow electrophoresis (μFFE) area, as well as gold microelectrodes for impedimetric monitoring, were deposited by sputtering and photolithographic structuring (SI Fig. S1B). For electric insulation, a polymer-based SU-8 passivation layer was applied in the microcavity-based detection area. For a tight seal, a glass plate with appropriately aligned vias for inlets and outlets, as well as openings for the microcavity structures, was bonded on top of the structured glass substrate (Fig. 1B–SI Fig. S1A,C) using polyethene glycol diacrylate (PEG-DA). Additionally, holes for bubble traps were incorporated into the top glass substrate, aligned with small bars in the synthesis loop (SI Fig. S1A,B), and covered with gas-permeable polydimethylsiloxane (PDMS) membranes for sealing (SI Fig. S1D).

For running the μFFE in an efficient and reliable way, a homogenous field distribution is needed, which could be achieved by a high-conductivity electrode buffer. Therefore, the electrode buffer streams must be separated from the running buffer reservoir by an electrically conductive hydrogel. This was achieved through the UV-light induced polymerization of PEG-DA containing 20 % water within the purification chamber (SI Fig. S1C). Furthermore, a 7 °- tilted surface for the platinum electrodes was etched into the glass, allowing the electrode material to be sputtered within the μFFE purification chamber and reliably connected electrically to the conducting tracks on the glass surface (SI Fig. S1A,B) and enlarging the homogeneous electric field for a more stable separation as shown by basic FEM simulation of the electric field (SI Fig. S2). While low-conductivity running buffers are advantageous for μFFE separations, they are detrimental to cells; therefore, the outlet flows must be conditioned with cell culture medium to restore physiological conditions and enable biosensing by sensitive cell culture models. Hence, meander-like channels, serving as passive mixing structures, were integrated into the three separation area compound outlets (Fig. 1B–SI Fig. S1A). For sensitive detection of bioactivity by 3D-cultures or organoids, microcavity structures with microelectrodes were incorporated into the glass substrate with integrated connections to the mixer outlet channels (Fig. 1B). The initial microcavity edge length of 400 μm (Fig. 1B) was chosen to cover a 3D culture size range of about 300–450 μm but could be adapted for other sizes if necessary. Using 3D cell cultures as a biosensing element in LOC devices always harbors the problem of correct positioning as simply and reliably as possible, especially in a microfluidic stream. To overcome this limitation, a PDMS adapter was designed with U-shaped channel guiding structures that, when correctly aligned on top of the microcavities (SI Fig. S1E), allow for easy positioning of 3D cell cultures or organoids in the microcavities and, moreover, reliable contact with the measurement electrodes on the microcavity walls. This last point is crucial for achieving a stable bioelectronic readout of 3D cell culture under flow conditions, such as impedance spectroscopy-based monitoring of human cardiomyocyte clusters (hCMC). The PDMS adapter with U-shaped guiding channels also allows for easy removing of the 3D cell cultures after the experiments for later reuse or further analysis.

Taken together, despite the complexity of integrating a whole process chain structure, as shown in Fig. 1A, on a single 8 cm × 8 cm chip, especially including the inline monitoring of bioactivity using 3D cell cultures, we managed to take into account all crucial points to develop and fabricate a holistic MiCAPSUiD system. With regard to the complex manufacturing process the MiCAPSUiD chip was designed as a reusable chip. In accordance with the chemical synthesis requirements for

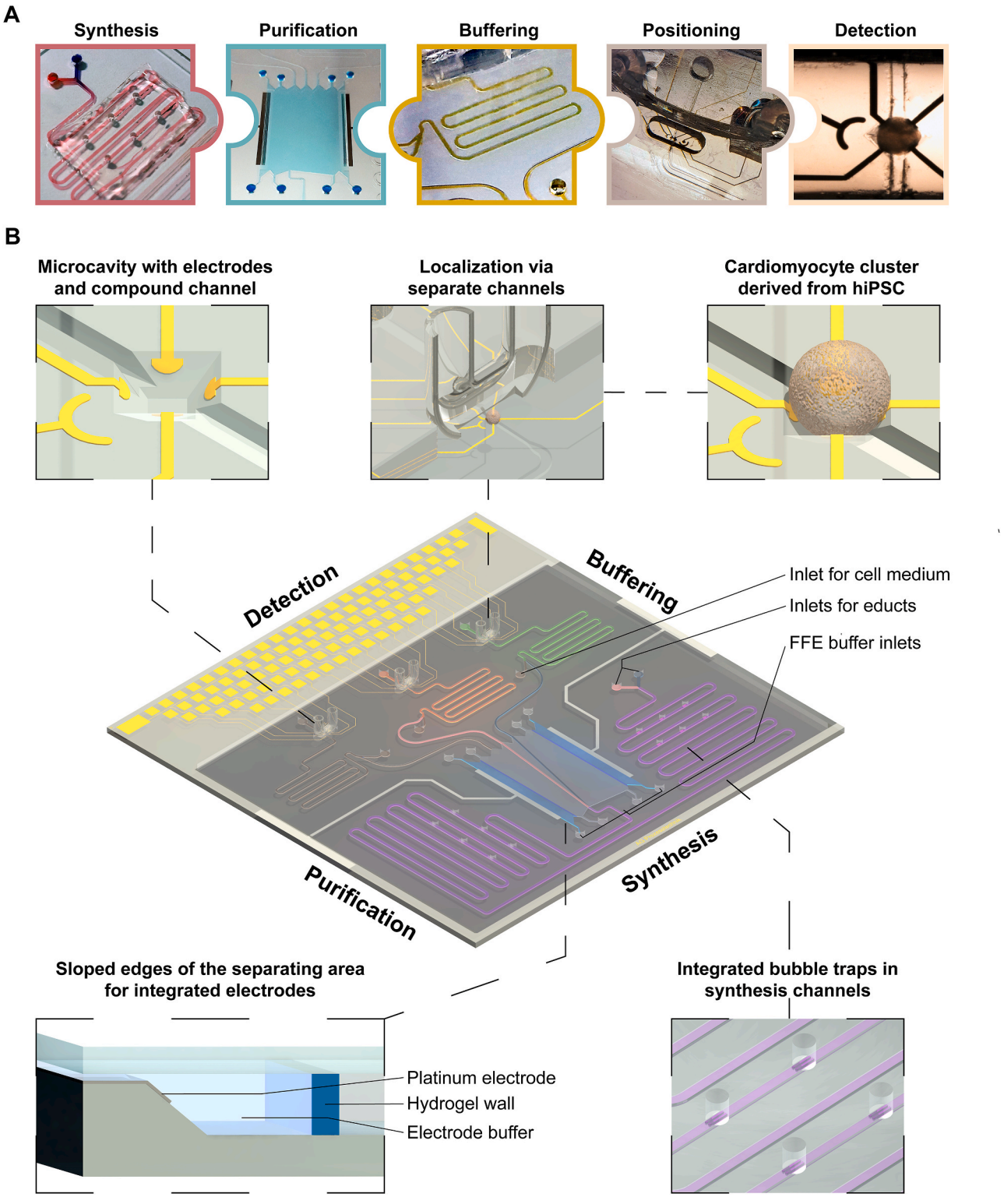

Fig. 1. Microfluidic chip concept for continuous compound synthesis, purification and impedimetric inline monitoring of bioactivity on 3D cultures. (A) Necessary process chain steps that were optimized and integrated in the microfluidic MiCAPSUiD. (B) Schematic representation of the microfluidic MiCAPSUiD setup including synthesis loop (violet) with two inlets, and integrated bubble traps, a purification area (total length of 2 cm) for continuous purification by micro free-flow electrophoresis (μFFE) as well as electrically conductive hydrogel walls and sloped side walls (detail view) for optimum platinum electrode integration and separation of high conductive electrode buffer streams. At the end of the purification area there are five outlets (two sheath stream outlets and three compound stream outlets). The compound outlets are connected to meander mixing structures, which buffer the compound stream to physiological conditions. Finally, the mixer outlets lead to the microcavity structures, which feature four microelectrodes and a counter/reference electrode (detailed view). For reliable positioning of 3D cultures into the microcavities, a PDMS block with incorporated round guiding channels is aligned on top of the microcavities (detailed view). (For interpretation of the references to color in this figure legend, the reader is referred to the Web version of this article.)

chemical stability and robustness, materials (glass, noble metals like platinum and gold) as well as build up processes were chosen with regard to easy and robust cleaning and reusability. Thus, MiCAPSUiD chips were used in several tests and experiments.

3.2. Continuous on-chip micro-flow synthesis of propranolol

For the proof of concept, we chose the chemical synthesis of the cardioactive compound propranolol from its oxirane precursor (Fig. 2A). To determine the yield, ^{1}H NMR spectroscopy was used. Since both the oxirane starting material and the product share the same methoxy-naphthyl backbone structure, many peaks in the spectra of the two pure substances overlap (Fig. 2B–SI Fig. S3). Nevertheless, the yield could be determined as the ratio of the peak integrals of the oxirane starting material and the product at a chemical shift of 8.20 for the precursor oxirane and at 8.25 for propranolol (Fig. 2B).

In the first batch experiments (SI Fig. S4A) at room temperature, a yield below 5 % was achieved, and even heating to 40 °C for 15 min resulted in just 17 % yield, which is likely due to the epoxide opening being a slow reaction under standard conditions. According to Cepanec et al., (2003), the use of the catalyst calcium trifluoromethanesulfonate dissolved in organic solvents such as acetonitrile (ACN) or dimethylsulfoxide (DMSO) enhances the epoxide ring opening. As a result, significantly higher yields were achieved with a 250 mM catalyst at room temperature, yielding 29 % with ACN and 36 % with DMSO as solvent (approximately 7-fold higher yield compared to initial attempts)

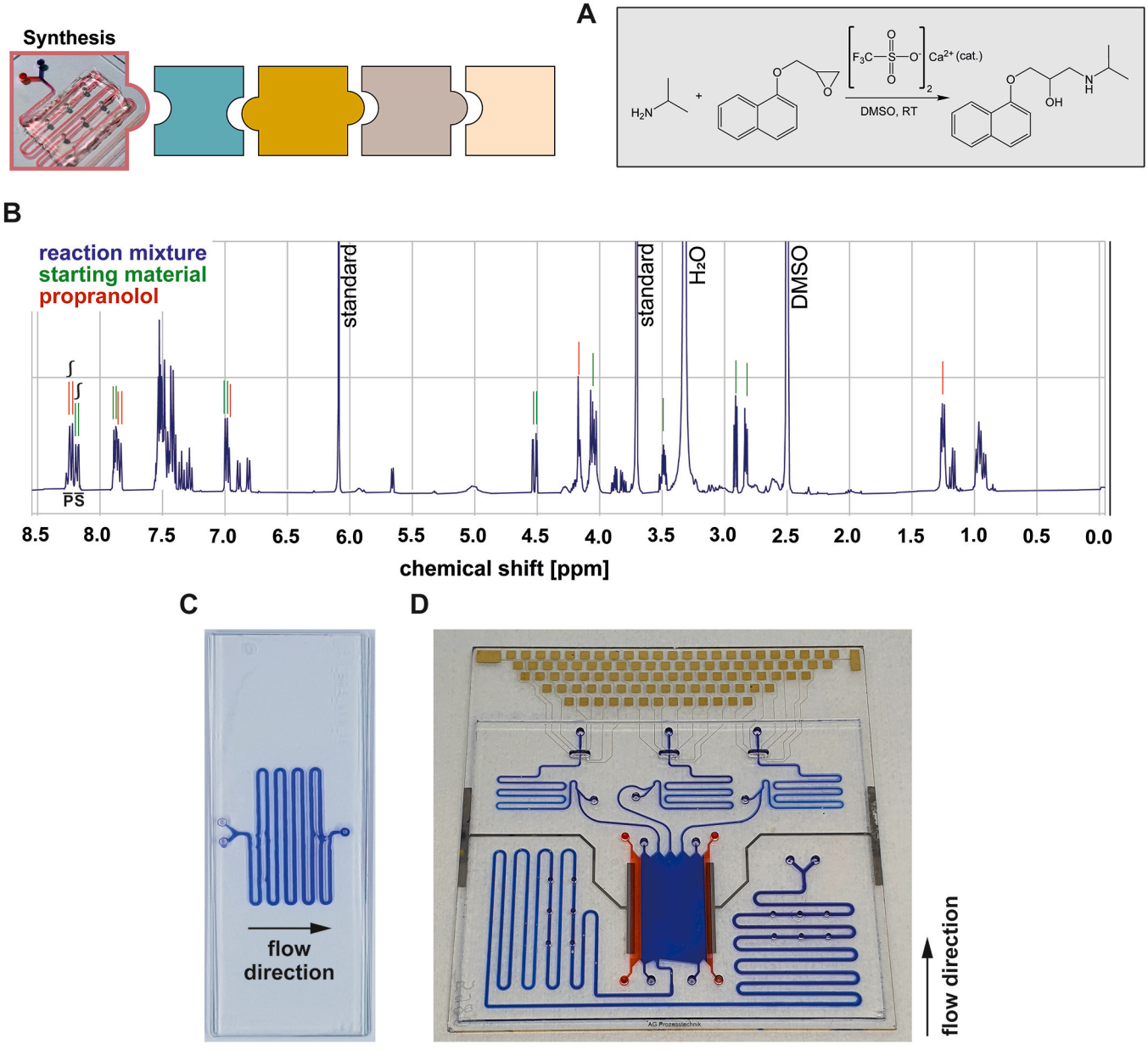

Fig. 2. Characterization of the on-chip continuous micro-flow propranolol synthesis. (A) Isopropylamine reacts with 2-(naphthalen-1-yloxy)methyl oxirane with the catalyst calcium trifluoromethanesulfonate in DMSO at room temperature (RT) to propranolol. (B) Exemplary ^{1}H NMR spectrum in d^{6}-DMSO for the yield determination. The yield equals the ratio of the peak area integrals of the chemical shift at 8.20 for the starting material (S) and at 8.25 for the propranolol product (P). Trimethylbenzene was used as an NMR standard. (C) Synthesis chip (blue ink,75 × 25 mm × 2.05 mm, synthesis loop length 241 mm). (D) The MiCAPSUiD (80 mm × 80 mm × 2 mm) contains a synthesis loop with a length of 563 mm. All microfluidic channels were filled with blue ink, except for the μFFE electrode buffer channels (separated by hydrogel walls), which are filled with red ink. (For interpretation of the references to color in this figure legend, the reader is referred to the Web version of this article.)

(SI Fig. S4A). Since DMSO as a solvent showed the highest yields, all further experiments were performed using DMSO.

For establishing the synthesis under microfluidic conditions, a synthesis chip (Fig. 2C) was fabricated in glass using the selective laser etching (SLE) technology, which is necessary for organic solvent resistance. The synthesis channel (dimensions: 130 μm × 500 μm × 24 cm) had a length of 241 mm. By controlling the flow rate, different reaction times (40 min and 80 min) were tested using 100 mM catalyst in DMSO at room temperature with a fourfold excess of isopropylamine. The catalyst concentration had to be lowered from initially 250 mM (SI Fig. S4A) to 100 mM (SI Fig. S4B) due to an adverse effect of high catalyst concentrations on the deflection efficiency in electrophoresis pre-tests (SI Fig. S5). The comparison of synthesis under microfluidic conditions to appropriate batch experiments revealed comparable yields after 40 min (29 % in batch *vs* 27 % in flow) and 80 min (59 % in batch and in flow) (SI Fig. S4B), which indicates that microfluidic synthesis efficiency is comparable to batch synthesis. Overall, the use of the catalyst calcium trifluoromethanesulfonate significantly increased the yields in the synthesis as described by Cepanec et al. (2003), enabling a successful propranolol synthesis within an hour instead of several days (Tran et al., 2020). In the context of upstream isolation and purification of a synthesized product from residual starting materials, the achieved yield rates are very well suited for demonstrating the proof-of-concept.

In the next step, the synthesis was integrated into the MiCAPSUiD system (Fig. 2D), which features a comparable synthesis loop geometry but a length of 563 mm, to achieve the appropriate upstream flow rates. For a reaction time of 50 min at room temperature, the micro-flow synthesis on the MiCAPSUiD system showed comparable yields to the corresponding batch experiment (32 % in flow *vs.* 28 % in batch) (SI Fig. S4B) and represents a good balance between yield and reaction time/temperature in comparison to previous described 70 % yield in batch synthesis for a reaction time of 48 h as well as 41 % (0 %) yield in microflow synthesis with a reaction time of 30 min at 100 °C (80 °C) (Angelis et al., 2019).

During the synthesis, it was clearly visible that the volatile isopropylamine, with a boiling point of 32 °C, evaporates on the chip, leading to bubble formation within the channels. Although this was not critical for the performed synthesis reaction so far, bubble formation in complex microfluidic systems can have a critical impact and is a widely known problem (Pereiro et al., 2019). In the present case, bubbles from the synthesis loop outlet caused distortions in the upstream purification by μFFE, prohibiting continuous deflection of the product for 10–30 min. In worst cases, the bubbles block the channels of the purification chamber or the current flow, thereby preventing the purification of the product.

To overcome this limitation, we use passive bubble traps (SI Fig. S6). The general idea is a flow-through device with a cavity for the bubbles and a barrier structure after the cavity to increase the fluidic resistance, thereby preventing the bubbles from simply flowing through the device. Therefore, barrier structures were integrated within the channels using SLE technology to increase the flow resistance and cause the bubbles to float up and be trapped in holes in the cover glass, which is sealed with a 230 μm-thin gas-permeable PDMS membrane. Thus, trapped bubbles in the cavity could escape the device through the PDMS instead of entering the μFFE purification chamber (SI Mov. S1). The bubble trap with a PDMS membrane works perfectly for small bubbles and was integrated into the MiCAPSUiD without problems. On the MiCAPSUiD, six bubble traps were placed near the synthesis inlets and six bubble traps shortly before the mixture enters the purification chamber, resulting in nearly complete bubble suppression at the synthesis loop outlet. Beside some tiny bubbles which were flushed through the entire system without any problem, there were no disturbance or even blocking at the downstream μFFE based purification due to larger bubbles over a time range of at least 1 h observable.

3.3. μFFE-based purification and re-buffering on the MiCAPSUiD

The product purification using μFFE, the subsequent buffering to physiological conditions and the effect on the hCMCs were first tested with a defined composition of 40 mM oxirane precursor and 60 mM propranolol in DMSO. Both compounds share the naphthalene backbone and show a fluorescence signal, when excited with a 266 nm laser. The μFFE based purification principle (SI Fig. S7) is based on the mixture that enters the purification chamber and flows through as a single peak, representing the flow towards outlet 2 in the electropherogram (Fig. 3A, 0 V). When applying a voltage, the single positive charged propranolol is deflected towards outlet 3, while the uncharged organic solvent DMSO and the oxirane precursor flow without deflection to outlet 2 (Figs. 3A and 18 V). For estimating the deflection efficiency, a two-Gaussian fit was applied to the electropherogram (SI Fig. S8). There, the deflection efficiency was determined to be 76.5 %, as 45.9 mM of the total 60 mM propranolol was deflected to outlet 3, which is in line with a previous study for μFFE based propranolol separation with an deflection efficiency of 75 % (Haensch et al., 2022). In a further experiment, a mixture of 100 mM propranolol and 25 mM oxirane precursor in DMSO was separated by μFFE. The amount of propranolol in the collected fluids at the outlets 2 and 3 were analyzed using mass spectrometry after 40 min with 1 μL/min flowrate (SI Fig. S9). The quantification revealed 34 % deflected propranolol in outlet 3. In contrast, 62 % was found in outlet 2 and 4 % in outlet 1. Observed differences in deflection efficiencies can be caused by variances and minor distortions in the μFFE-based stream alignments, especially within long-time running's. This is supported by the observed portion of 4 % in outlet 1. Furthermore, an increased amount of propranolol can lead to lowered deflection efficiency and would need an optimization of the μFFE purification chamber to overcome this. With a focus on integrating the biosensor approach, we limited the maximum concentration of propranolol to 60 mM in following experiments.

Due to the requirement of a hypotonic running buffer for μFFE (5 mM phosphate buffer), all μFFE outlet streams need to be buffered to physiological conditions and must be diluted in cell-compatible culture medium. For this purpose, different mixture structures, such as fishbone-like mixing structures (Nguyen and Wu, 2005) (SI Fig. S10A) with lengths of 22–44 mm and meander-like mixing structures (SI Fig. S10B) with varying lengths from 75 to 130 mm, were testes with a fluorescein/rhodamine B mixture. The overall aim for the mixing structure was to take up as little area as possible on the chip and apply as little back-pressure as possible. While the shortest meander-like mixing structure (75 mm) revealed a highly suitable mixing performance, the longest tested fishbone-like mixing structures (with comparable needed area on the chip and wider channels for lower back-pressure) only showed an insufficient mixing capability (Fig. 3B). Based on these results, we integrated meander-like mixing structures with a length of 83 mm on the MiCAPSUiD system for each of the three μFFE outlet channels. Next, we identified optimum mixing ratios to achieve maximum cell compatibility and contraction functionality of the hCMC cultures with regard to stable contraction rates. Therefore, a constant flow rate of 20 μl/min with 5 mM phosphate buffer was applied at the inlet of the μFFE chamber that resulted in a 6.7 μL/min flow rate at each of the three symmetrical μFFE outlets. This outlet flow was mixed with a varying flow rate of the cardiomyocyte culture medium, ranging from 5 to 15 μL/min. The mixed streams were collected at the outlets and applied to six hCMC per mixture in a 96-well plate, with the standard culture medium used as a control. Since the contraction rate is a very sensitive parameter of cardiomyocyte cultures concerning environmental changes for example the buffer concentration, the contraction of each hCMC was counted manually by microscopic observation at different time points (Fig. 3C). The relative values normalized to the control (only standard cell culture medium) revealed high variances for lower proportion of cell culture medium in the buffer with dynamically increases up to 160 % after 10 min (5 μL/min) down to about 65 % after 10 min

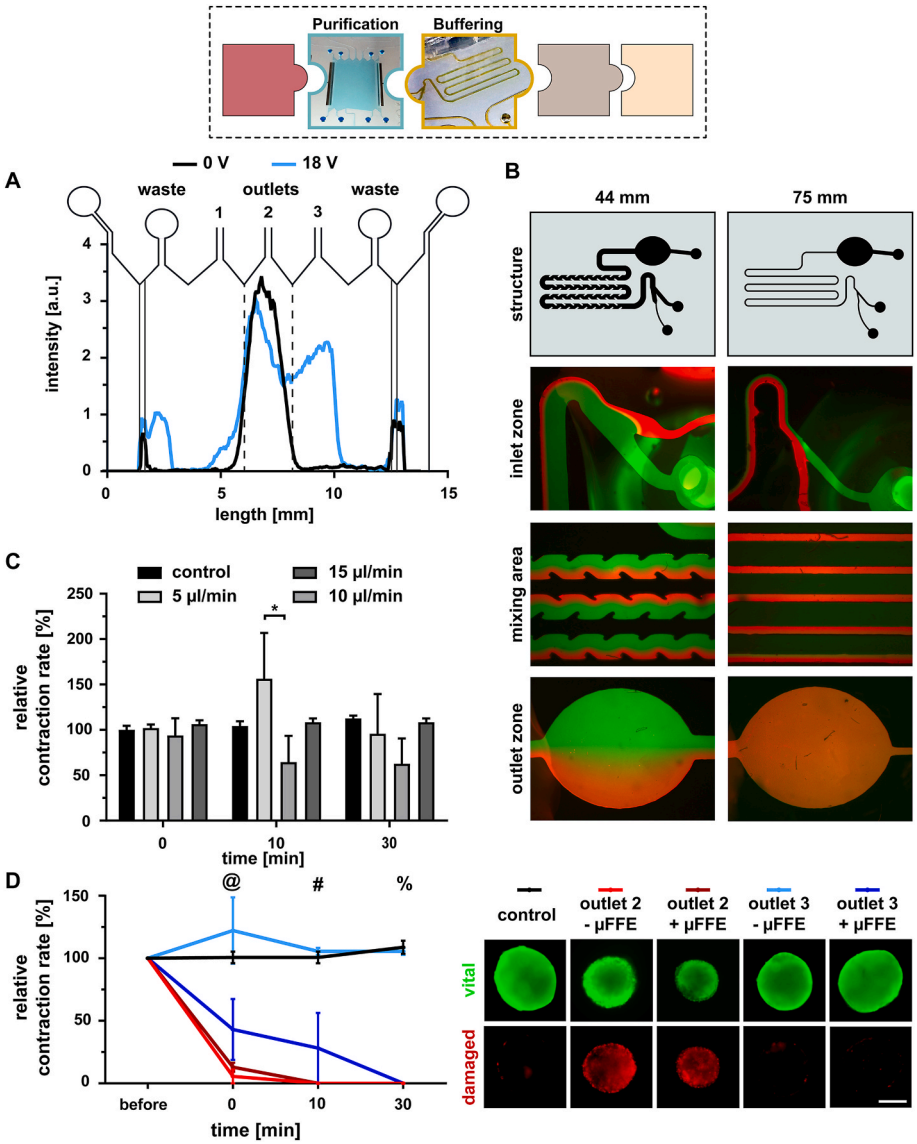

Fig. 3. Purification, mixing and cellular detection of the product propranolol. (A) Electropherograms of the sample collection after µFFE of a 40 mM precursor/60 mM propranolol mixture in DMSO without a voltage (black) and with an applied voltage of 18 V (blue, 400 µA). (B) Comparison of 44 mm fishbone-like mixers and 75 mm meander-like mixers. (C) Mixing of 5 mM phosphate buffer with different flow rates of standard culture medium. A 20 µL/min flow of phosphate buffer was applied to the purification chamber. Each of the three outlets was buffered with medium of 5–15 µL/min, and the mixtures were collected. Furthermore, hCMCs were placed in the buffer mixtures in a 96-well plate, and the contractions within a 30-s time frame were counted optically. Standard culture medium was used as a control (mean ± sem, n = 6 hCMCs per condition). Data were normalized to the "0 min control" value. *$p \leq 0.05$ (D) Organoid behavior on the different outlet flows without (−) or with (+) a voltage applied in the µFFE. The flow of the mixture of 40 mM oxirane precursor and 60 mM propranolol product was collected after buffering with 15 µL/min standard culture medium and tested on organoids in a 96-well plate, followed by a live-dead staining with calcein AM (green, vital) and propidium iodide (red, damaged) (scale 200 µm). The contractions were evaluated optically. Standard culture medium was used as control (mean ± sem, n = 3 organoids per condition). Data were normalized to the value before the measurement. **@:** control *vs.* outlet 2 before µFFE, outlet 2 with µFFE: ***; control *vs.* outlet 3 with µFFE: **; outlet 2 before µFFE *vs.* outlet 3 before µFFE: ***; outlet 2 with µFFE *vs.* outlet 3 before µFFE: ***; outlet 3 before µFFE *vs.* outlet 3 with µFFE: *** **# and %:** control *vs.* outlet 2 before µFFE, outlet 2 with µFFE, outlet 3 with µFFE: ***; outlet 2 before µFFE *vs.* outlet 3 before µFFE: ***; outlet 2 with µFFE *vs.* outlet 3 before µFFE: ***; outlet 3 before µFFE *vs.* outlet 3 with µFFE: *** **$p \leq 0.01$ ***$p \leq 0.001$. (For interpretation of the references to color in this figure legend, the reader is referred to the Web version of this article.)

(10 µL/min). These high contraction rate variances are understandably caused by an excessive proportion of hypotonic buffer which effects the ion homeostasis of the hCMCs. In contrast, the mixture with a flow rate of 15 µL/min culture medium (ratio of 1:2.2) was sufficient to achieve comparable contraction stability to the control and was therefore chosen for the following experiments.

Next, the outlet flows from the µFFE (Fig. 3A) with the defined composition of 40 mM oxirane precursor and 60 mM propranolol in DMSO were tested on the hCMCs (Fig. 3D). Therefore, the outlet flows from the outlets 2 and 3 were collected either with or without running the µFFE and exposed to three hCMCs per condition in a 96-well titerplate. The contractions were counted by microscopic observation before the hCMCs were placed in the conditioned medium, directly after transfer to the conditioned medium as well as 10 min and 30 min later. Afterwards, the hCMCs were stained with calcein AM and propidium iodide for live and dead cells. Control hCMCs exhibited nearly unchanged contraction rates and no dead cells. When transferring the hCMCs in the flows from outlet 2, a rapid and highly significant decrease in relative contraction rate, down to about 10 % compared to the control, was observed for both conditions with and without running the

μFFE, and a complete stop of contractions occurred after 10 min. Additionally, the live-dead staining revealed lots of damaged cells. This can be attributed to the toxic effect of the oxirane precursor and the high DMSO concentrations that flow toward outlet 2 during the product purification. This toxic effect was further investigated using a tetrazolium cytotoxicity assay according to ISO 10993-5 (SI Fig. S11). At 100 μM, the precursor oxirane and DMSO concentrations of 5 % and higher are considered toxic.

hCMCs incubated in the conditioned medium of outlet 3 without μFFE, yielded values comparable to the control after 10 min. In contrast, hCMCs incubated in the conditioned medium of outlet 3 with μFFE, resulted in a significantly decreased contraction rate, down to 40 % with a subsequent decrease to 30 % after 10 min and no contractions after 30 min, without showing damaged cells in the live-dead staining. This is evidence that the decline in contraction rate is due to the pharmacological effect of propranolol. In line with this result, the field potential analysis revealed a decreasing contraction rate in static measurements on hCMCs (SI Fig. S12), while no toxic effect was observed up to 1 mM propranolol (SI Fig. S11). Furthermore, the determined IC_{50} value of about 6.7 μM for the negative chronotropic effect of propranolol is in

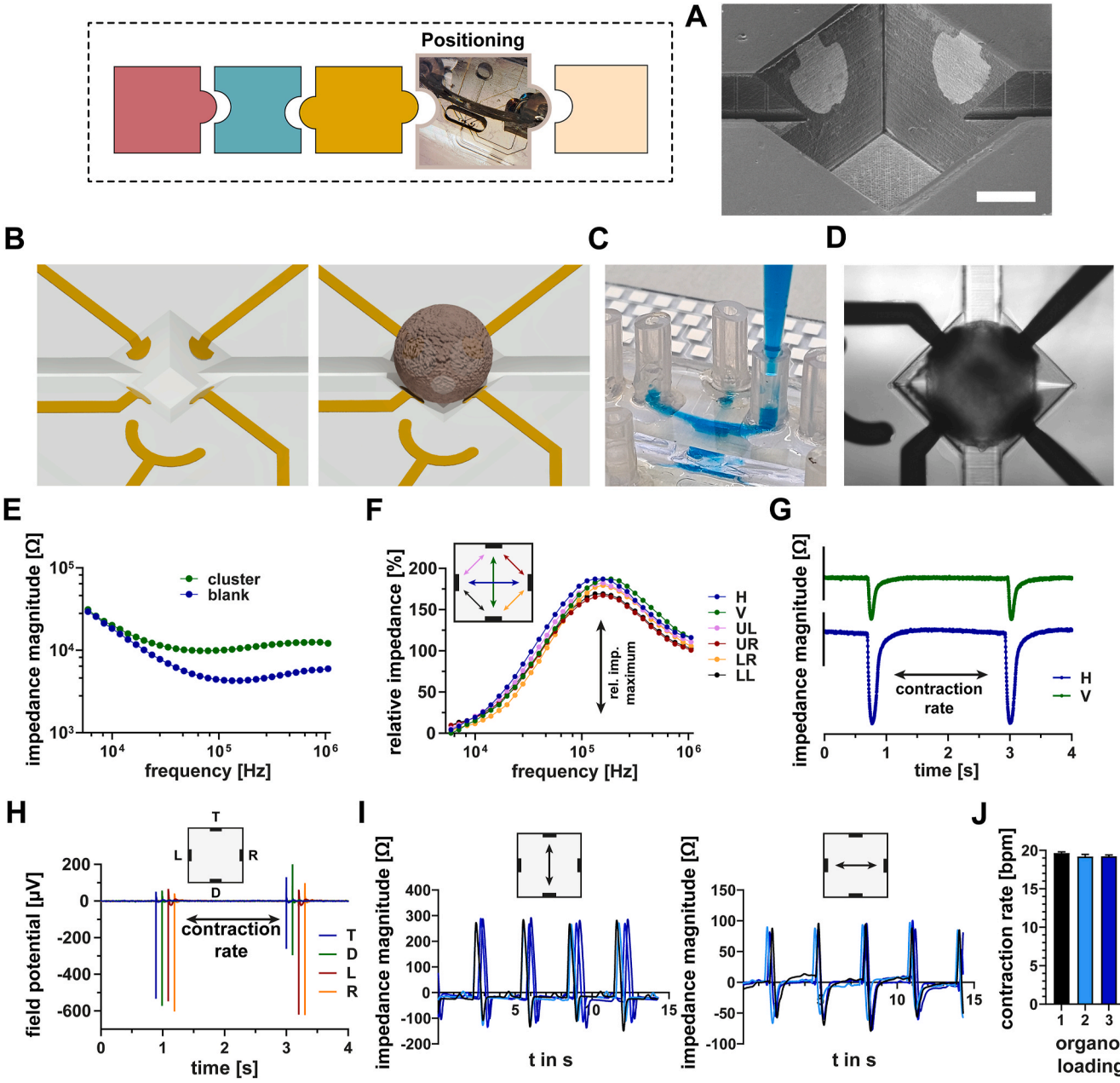

Fig. 4. hCMC positioning and bioelectronic signal characterization under flow conditions. (A) SEM image of the microcavity with integrated microchannel (scale bar 100 μm). (B) Schematic illustration of the microcavity without and with a hCMC. (C) Positioning of hCMC into the microcavity by pipetting the hCMC through the PDMS guiding channel (blue colored). (D) Microscopic image of perfectly positioned hCMC within a microcavity of the MiCAPSUiD system. (E) Impedance magnitude spectra from empty and cluster loaded microcavity. (F) Calculated relative impedance spectra (cluster signal) for all possible electrode combinations of the perfectly positioned hCMC with maximum impedance signal at around 100 kHz. (G) Impedance magnitude time trace at 100 kHz revealing characteristic peak signals caused by mechanical contraction. (H) Field potential recording from all 4 electrodes for the same hCMC with typical action potential derived peaks (electrode signal traces are shifted by 100 ms for better visualization). (I) Impedance magnitude time trace signals of repeated hCMC positioned in the same microcavity for 4 times. (J) Statistical analysis of determined contraction rate for the positioned hCMC (mean ± sem, n = 4 positionings). (For interpretation of the references to color in this figure legend, the reader is referred to the Web version of this article.)

line with studies on atrial rat cardiomyocytes (IC_{50} 16 μM, Oliveira et al., 2025) as well as hiPSC derived 2D cardiomyocyte cultures (IC_{50} 1–10 μM, Honda et al., 2021) and is in the *in vivo* relevant therapeutic window that is in the low micromolar range (Pasquier et al., 2011).

3.4. hCMC positioning in the MiCAPSUiD system and bioelectronic signal characterization under flow conditions

For the biosensoric inline monitoring of the μFFE outlet flows, microcavities with microelectrodes on the side walls (Fig. 4A, SI Fig. S13) were integrated comprising a microchannel that is connected to the μFFE outlet (Fig. 4B). The quality of the microelectrodes can be examined very well by impedance spectroscopy. With regards to the reusability, we examined MiCAPSUiD chips over 5 experiments without microelectrode degeneration (SI Fig. S14). Next, we demonstrated the hCMC positioning into the microcavities by using the optimized PDMS guiding channel that is covalently bonded on top of the microcavities. The hCMCs were either loaded directly into the channel by simply pipetting or by connecting a hCMC-containing hose with a syringe (Fig. 4C). For a perfect and robust positioning, microcavities had an edge length of 400 μm. hCMCs with a diameter in the range of 380–400 μm in diameter are preferred. Due to a single cluster generation per well, the size can be precisely controlled by the initial cell seeding number (SI Fig. S15). When a hCMC is perfectly positioned in a microcavity (Fig. 4D), impedance spectra can be recorded for all 6 electrode combinations and the hCMC signal can be extracted as relative impedance spectra (Fig. 4E and F). Since suboptimal positioned hCMC can be easily identified using these spectra (SI Fig. S16) or even complete flushing away under flow condition, impedance spectroscopy is a perfect method for inline monitoring of positioning. More strikingly, using a high precision impedance analyzer with sufficient speed (>300 samples/s) around the frequency where the cluster signal is maximal (100 kHz), the recorded impedance magnitude time trace can provide highly resolved peak signals that are caused by the mechanical contraction of the hCMC (Fig. 4G) and can be used to determine the peat-to-peak interval and therefore, the contraction rate. Additionally, using our self-developed multimodal bioelectronic monitoring platform, field potential can also be recorded to investigate in the electrophysiology of hCMCs (Fig. 4H). The contraction rate can therefore also be determined based on the typical peaks caused by action potentials.

In a next experiment, the signal reproducibility and stability were investigated with a hCMC being removed and repositioned several times monitored by impedance magnitude time trace (Fig. 4I) that revealed highly comparable contraction peak signals. The statistical analysis of the determined contraction rates (Fig. 4J) revealed no significant changes over the 4 (re)positioning attempts. The simple and robust positioning of 3D cultures in seconds under flow conditions represents a significant improvement over 2D cell cultures in (micro)fluidic chips that need days for establishment and don't allow an easy exchange (Zitzmann et al., 2017a).

Additionally, we wanted to demonstrate the ability to monitor and quantify the chronotropic effect of propranolol under flow condition. Therefore, we positioned hCMCs in the MiCAPSUiD system and applied a continuous flow (20 μl/min) with increasing concentrations of propranolol through the microchannels that were integrated into the microcavities. Field potentials were recorded for 10 min (SI Fig. S17A) comparable to the static experiments. Due to the stable and high action potential signal amplitudes, the contraction rates could be robustly calculated and a concentration-response curve fitting revealed an IC_{50} value of 8.9 μM (SI Fig. S17B) that nicely fits to the value of 6,7 μM from the static setup (SI Fig S12C).

Overall, for the tested flow regime up to 50 μl/min, the field potential derived action potential as well as the impedimetric time trace derived contraction signals showed a high stability as well as amplitudes and SNR under flow conditions that are comparable to signals from the static setup previously described (Zitzmann et al., 2024). More strikingly, we did not see disturbing effects on the hCMC signal when the whole flow regime as well as the μFFE potential field was applied on the MiCAPSUiD system.

3.5. Impedance spectroscopy-based inline monitoring of bioactive effect of propranolol on human cardiomyocyte clusters (hCMC)

To demonstrate the combined process chain on the MiCAPSUiD system, the synthesis was performed with 100 mM catalyst dissolved in DMSO, using a fourfold excess of isopropylamine and a combined flow rate of 1 μL/min. For buffering the analytes after the μFFE, standard culture medium was used at a flow rate of 15 μL/min. The μFFE deflection-based product purification was performed for 60 min, showing a significantly different electropherogram (SI Fig. S18). In the samples taken from outlet 2 and 3 during the deflection, almost no propranolol or precursor oxirane was detectable. Instead, a white precipitate fell out. When rinsing the chip with 70 % ethanol solution in water, the white precipitate can be dissolved. NMR analysis of the precipitate revealed equal amounts of propranolol and oxirane (SI Fig. S19). This suggests that both components interact with either the isopropylamine or the catalyst, precipitating out of solution. As isopropylamine gets protonated in contact with the aqueous buffer, the solution becomes strongly alkaline, which may be the reason propranolol, which is usually single positively charged in water at pH 1–8, becomes deprotonated and starts to precipitate. The precursor oxirane is poorly water soluble and therefore may precipitate out of solution when used in high concentrations. Furthermore, the calcium ions of the catalyst come into contact with the phosphate ions (buffer) and may also contribute to the observed precipitation. Although this limitation highlights the challenges of complex process chains in microfluidic lab-on chip approaches, we used defined mixture of 40 mM oxirane and 60 mM propranolol in DMSO, without the catalyst and isopropylamine, to demonstrate inline biosensing with hCMCs for the bioactive effect of propranolol. Thus, with the targeted dilution factor of 1:15 due to the μFFE-based purification (Haensch et al., 2022) and the 1:2.2 mixing ratio with culture medium, the final concentration of propranolol is in the range of 1 mM, which is clearly above the determined IC_{50} value of 6.7 μM (static) to 8.9 μM (fluidic) and therefore high enough for a distinct propranolol negative chronotropic effect (SI Fig. S12), but below a toxic concentration (SI Fig. S11).

For the final combined process demonstration of the μFFE based propranolol deflection and purification, the rebuffering with cell culture media and the hCMC based impedimetric monitoring of the bioactive effect of propranolol, we had to ensure the long-term contraction signal stability. Since cardiomyocyte contraction is highly sensitive to environmental changes such as temperature (SI Fig. S20), we ensured constant 37 °C for the whole experiments by a self-developed active controlled heater that was integrated in the microscopic chip holder below the microcavity region. After hCMCs were positioned in the microcavities of the MiCAPSUiD system, impedance magnitude time traces were acquired over a period of 3 h at 100 kHz (Fig. 5A) proving the long-term stability of the hCMC contraction signal as well as the contraction rate.

Therefore, the final experiments were started with positioning of hCMCs in the appropriate microcavities for the different outlets. To obtain a stable baseline, hCMCs were perfused with only culture medium as control for approximately 20 min (Fig. 5B). Afterwards, the flow from the μFFE outlets was led over the hCMCs. The first effect of the deflected propranolol at outlet 3 could be observed after 8–15 min with a decrease from 15 bpm down to 10 bpm and finally a complete stop of the contraction after 14 min. In contrast, the flow from outlet 2 led to complete contraction signal diminishing within the first 8 min. According to observations from the initial μFFE functional test experiments (Fig. 3D) this is caused by the cytotoxic effect of the toxic oxirane precursor and toxic solvent concentrations. This could also be proved again by microscopic live/dead staining after experiment end (Fig. 5C). For

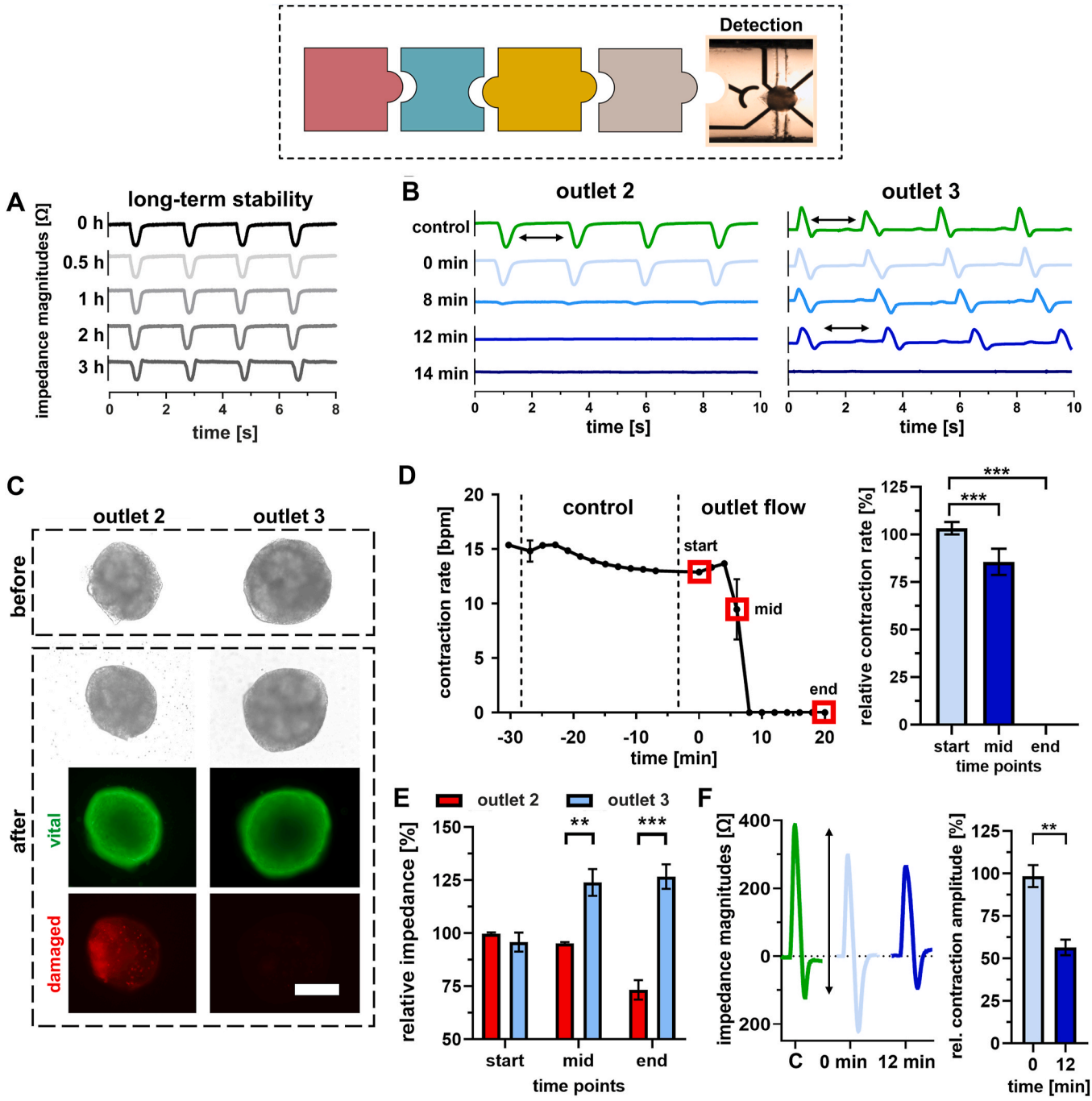

Fig. 5. Impedimetric inline monitoring of the biological effect of propranolol on hCMCs. (A) hCMCs were positioned in the microcavities on the chip and perfused with only standard culture medium for 3 h to demonstrate baseline long-term stability of impedance magnitude trace derived contraction signals at 100 kHz. Exemplary impedance magnitude traces of one electrode are shown. (B) For the detection experiment a baseline signal was obtained (control). Afterwards, flow from outlet 2 (containing DMSO + oxirane precursor) as well as flow from outlet 3 (containing deflected propranolol) were directed over the hCMCs. Exemplary impedance magnitude traces of one electrode from outlet 2 and outlet 3 are shown. (C) Microscopic images of hCMC before and after the experiment including a live-dead staining with calcein AM (green, vital) and propidium iodide (red, damaged) (scale 200 μm). (D) Determined contraction rate trace for one hCMC (mean ± sem, n = 3 electrode combinations) and the relative contraction rate at different time points (red squares) normalized to the control baseline (mean ± sem, n = 3 hCMC from 3 independent experiments/chips, ***p ≤ 0.001). (E) Relative impedance (cell signal) of the hCMCs at different time points normalized to the control baseline (mean ± sem, n = 3 hCMC from 3 independent experiments/chips, **p ≤ 0.01 ***p ≤ 0.001). (F) Exemplarily impedance magnitude trace derived contraction signals from outlet 3 (control, 0 min, 12 min) and statistical analysis of signal amplitudes normalized to the control baseline (mean ± sem, n = 3 hCMC from 3 independent experiments/chips, **p ≤ 0.01). (For interpretation of the references to color in this figure legend, the reader is referred to the Web version of this article.)

quantitative analysis of the purified propranolol, the contraction rates were determined for the outlet 3 hCMC from 3 electrode combination signal traces (Fig. 5D). For demonstrating reproducibility of the observed effect, 3 independent experiments with 3 different MiCAPSUiD chips were performed, prominent time points were selected, and the contraction rate values were normalized to the base line (control) for each experiment. The statistical analysis of the negative chronotropic propranolol effect revealed a distinct decrease of the contraction rate

down to 58.6 ± 6.8 % at mid and a significant reduction to zero contraction at the end time point.

To demonstrate that the observed effect is the chronotropic effect of propranolol and is not caused by negative (cytotoxic) side effects, we analyzed the cluster signal represented by calculating relative impedance values using recorded blank values (without hCMCs). The flow from outlet 3 resulted in an increase in relative impedance up to 126.7 ± 8.5 % (Fig. 5E), which cannot be correlated with cardiotoxic effects (Krinke et al., 2009; Schmidt et al., 2021). We did not expect this effect, but looking at the *in vivo* pharmacology of propranolol beyond the negative chronotropic effect, there is also a negative inotropic effect meaning a reduced tissue tension for our *in vitro* situation that would lead to a more relaxed cardiomyocyte spheroidal cluster. The cluster can then lay more smoothly onto the geometry and electrodes of the microcavity and thereby could lead to an increased relative impedance signal of the hCMC. For verification, comparable experiments were performed in a static microcavity setup in a cell incubator environment (SI Fig. S21) that revealed a comparable impedance increase. Additionally, the weakening in the contraction force should also be visible in the impedance magnitude trace derived contraction peak signal amplitudes (Fig. 5F). The statistical analysis from the 3 independent experiments revealed a significant contraction peak amplitude reduction down to 56.5 ± 4.6 % after 12 min. This strongly supports the assumption that the observed effect of an increased relative impedance signal is caused by the negative inotropic effect of propranolol. In contrast, the flow from outlet 2, containing cytotoxic amounts of organic solvent and starting material, led to significantly decreased relative impedance values down to 73.3 ± 4.6 %, indicating a degeneration of the cells and cluster structure due to a cytotoxic effect that is in line with the live/dead staining (Fig. 5C).

Taken together, the integrated inline monitoring using impedance spectroscopy revealed the non-cytotoxic, negative chronotropic effect of propranolol on outlet 3, as well as the cytotoxic side effects of the oxirane precursor and the organic solvent DMSO on outlet 2. Furthermore, the potential negative inotropic effect of propranolol could also be observed by impedimetric monitoring. Thus, the microcavity-based impedance spectroscopy monitoring of bioactive drug effects on cardiomyocyte 3D cultures was successfully demonstrated.

4. Conclusion

In this study, we demonstrate, for the first time, the integration of a non-invasive, label-free, inline monitoring system for biological activity on 3D cardiomyocyte cultures using multiparametric impedance spectroscopy in a microfluidic chip approach for continuous chemical synthesis and upstream purification. In detail, we demonstrate for the first time the functional integration of microfluidic channels in microcavities for biosensoric applications and as a prerequisite for this, the capability for robust bioelectronic monitoring of spheroidal 3D cultures (hCMC) in a continuous flow setup by impedance spectroscopy and field potential recording without any disturbance by the applied flow regime as well as the μFFE electric field. Furthermore, we demonstrated successfully the quantitative multiparametric monitoring of chronotropic and inotropic drug effects with a comparable IC_{50} value to a static setup as well as non-cytotoxicity and cytotoxic side effects by multimodal monitoring in a continuous flow setup at the same time. To the best of our knowledge, this is the first demonstration of a cell culture based biosensoric integration downstream of an on-chip synthesis and purification module on the same compact chip for a continuous flow application approach.

In this context, after testing and optimization of the individual modules for each step, we designed and fabricated the MiCAPSUiD chip with all modules integrated. Finally, we successfully demonstrated the functionality of all parts of the MiCAPSUiD system using the chosen synthesis reaction and purification example of the cardioactive drug propranolol. By doing so, we created a real-life situation on the MiCAPSUiD system with a catalyst-based continuous microflow synthesis, resulting in incomplete turnover and residual starting material, as well as high, cytotoxic concentrations of the organic solvent DMSO, along with a high risk of bubble formation due to the volatile starting material. By integrating bubble traps and continuous μFFE-based product purification as well as solvent separation, we were able to overcome these problems. Additionally, the integration of robust rebuffering and microcavity arrays in the microflow streams enabled non-invasive, label-free impedimetric inline monitoring of the bioactive effect of the chosen synthesis product, propranolol, using cardiomyocyte 3D cultures. Moreover, the multiparametric impedance spectroscopy based analysis nicely demonstrate the differential detection of cytotoxic side effects of residual starting material/solvent flow (μFFE outlet 2) vs. purified product flow (μFFE outlet 3) with no cytotoxic effect.

Taking the on-chip synthesis as the time limiting step into account with 50 min for the demonstration, the whole process of downstream purification (3 min), rebuffering (1 min) and hCMC based bioactivity testing (10–20 min) is performed in less than 70 min, which represents a huge saving in time and effort in comparison to batch synthesis, purification and analysis approaches that need a couple of hours or even days. On the basis of an input flow of 50 μg/min starting material the received amount of purified propranolol of about 7 μg/min on the μFFE outlet was diluted down to concentrations of about 1 mM in the sub-cytotoxic but maximum drug effect range. With regard to the whole synthesis to bioactivity test duration this means a starting material consumption in the range of about 3 mg (per hour) and a purified product amount in the range of about 0.4 μg propranolol (per hour) that is sufficient to analyze the maximum drug effect. This represents a significant material saving compared to typical minimum batch approaches with several gram of starting material as well as purified product for offline analysis. Even though we only tested a single propranolol concentration in the maximum drug effect range, the continuous flow approach within all steps/modules would also allow a quantification/concentration-response analysis by applying a sequence of different dilution steps according to the cumulative static experiment approach (see SI Fig. S12). This could be simply realized by variation of the μFFE outlet and rebuffering/medium flow ratio in future applications. In terms of scalability, the compact single-chip solution not only offers significant time and material savings, but enables significantly easier parallelization. With at least 6 necessary pumps for the symmetric flow regime and a microscope setup for positioning control and μFFE monitoring (if necessary), parallel operation of multiple MiCAPSUiD systems is feasible.

Although the development of complex lab-on-chip applications quickly reaches its limits in terms of practical implementation when cell-based analytics are to be integrated, our study demonstrates in a first proof-of-concept the capabilities and analytical advantages of integrating cell-based biosensing, even for 3D cultures of highly functionalized cells, such as cardiomyocytes, in complex lab-on-chip approaches. In this sense, our MiCAPSUiD proof-of-concept study may contribute to paving the way for the use of cell-based biosensing approaches in drug development, testing, and even diagnostic applications.

CRediT authorship contribution statement

T. Haensch: Writing – original draft, Methodology, Investigation. **F. D. Zitzmann:** Writing – original draft, Methodology, Investigation. **S. Schmidt:** Writing – review & editing, Methodology, Investigation. **C. Stanko:** Writing – review & editing, Investigation. **E. Paternoga:** Writing – review & editing, Methodology, Investigation. **M. Meier:** Writing – review & editing, Supervision, Resources. **K. Zeitler:** Writing – review & editing, Supervision, Methodology, Funding acquisition. **D. Belder:** Writing – review & editing, Supervision, Funding acquisition, Conceptualization. **A.A. Robitzki:** Writing – review & editing, Supervision, Resources, Funding acquisition, Conceptualization. **H.-G. Jahnke:** Writing – original draft, Supervision, Project administration, Investigation, Data curation, Conceptualization.

Declaration of competing interest

The authors declare that they have no known competing financial interests or personal relationships that could have appeared to influence the work reported in this paper.

Acknowledgements

This work was funded by the German Research Foundation (DFG, FOR RO 2652/2-2; ZE 717/8-1) and the European Union (EFRE) and the Saxon Ministry of Science and the Fine Arts (SMWK, project: "CardioEpiX", Grant No. 100685579). The impedance analyzer and confocal microscope were acquired with funds from the Free State of Saxony (SMWK) and the European Union (EFRE) (grant number: 100185265). We thank Marie van der Loh for assistance during the mass spectrometry measurements, Maximilian Blaha for the laser setup support and Winnie Weigel for assistance with cell cultivation.

Appendix A. Supplementary data

Supplementary data to this article can be found online at https://doi.org/10.1016/j.bios.2025.118256.

Data availability

Data will be made available on request.

References

Angelis, S. de, Celestini, P., Purgatorio, R., Degennaro, L., Rebuzzini, G., Luisi, R., Carlucci, C., 2019. J Flow Chem 9 (4), 231–236.
Capaldo, L., Wen, Z., Noël, T., 2023. Chem. Sci. 14 (16), 4230–4247.
Cepanec, I., Litvić, M., Mikuldaš, H., Bartolinčić, A., Vinković, V., 2003. Tetrahedron 59 (14), 2435–2439.
Crowther, A.F., Smith, L.H., 1968. J. Med. Chem. 11 (5), 1009–1013.
Das, A., Weise, C., Polack, M., Urban, R.D., Krafft, B., Hasan, S., Westphal, H., Warias, R., Schmidt, S., Gulder, T., Belder, D., 2022. J. Am. Chem. Soc. 144 (23), 10353–10360.
Gutmann, B., Cantillo, D., Kappe, C.O., 2015. Angew. Chem. 54 (23), 6688–6728.
Haensch, T., Zitzmann, F.D., Jahnke, H.-G., Blaha, M.E., Paternoga, E., Zeitler, K., Belder, D., Robitzki, A.A., 2022. ACS Sens. 7 (12), 3906–3914.
Hao, N., Nie, Y., Closson, A.B., Zhang, J.X.J., 2019. J. Colloid Interface Sci. 539, 87–94.
Hasan, S., Blaha, M.E., Piendl, S.K., Das, A., Geissler, D., Belder, D., 2022. Anal. Bioanal. Chem. 414 (1), 721–730.
Hessel, V., Mukherjee, S., Mitra, S., Goswami, A., Tran, N.N., Ferlin, F., Vaccaro, L., Galogahi, F.M., Nguyen, N.-T., Escribà-Gelonch, M., 2024. Green Chem. 26 (18), 9503–9528.
Honda, Y., Li, J., Hino, A., Tsujimoto, S., Lee, J.-K., 2021. Front. Pharmacol. 12, 680618.
Hu, Y., Liu, B., Wu, Y., Li, M., Liu, X., Ding, J., Han, X., Deng, Y., Hu, W., Zhong, C., 2020. Front. Chem. 8, 579828.
Jezierski, S., Klein, A.S., Benz, C., Schaefer, M., Nagl, S., Belder, D., 2013. Anal. Bioanal. Chem. 405 (16), 5381–5386.
Kaiser, C., Jen, T., Garvey, E., Bowen, W.D., Colella, D.F., Wardel, J.R., 1977. J. Med. Chem. 20 (5), 687–692.
Krinke, D., Jahnke, H.-G., Pänke, O., Robitzki, A.A., 2009. Biosens. Bioelectron. 24 (9), 2798–2803.
Li, G., Liu, C., Zhang, X., Zhai, P., Lai, X., Jiang, W., 2023. Biosens. Bioelectron. 228, 115187.
Liu, Y., Sun, L., Zhang, H., Shang, L., Zhao, Y., 2021. Chem. Rev. 121 (13), 7468–7529.
Mc Veigh, M., Bellan, L.M., 2024. Lab Chip 24 (5), 1226–1243.
Mende, M., Tsouka, A., Heidepriem, J., Paris, G., Mattes, D.S., Eickelmann, S., Bordoni, V., Wawrzinek, R., Fuchsberger, F.F., Seeberger, P.H., Rademacher, C., Delbianco, M., Mallagaray, A., Loeffler, F.F., 2020. Chem. Eur J. 26 (44), 9954–9963.
Morodo, R., Gérardy, R., Petit, G., Monbaliu, J.-C.M., 2019. Green Chem. 21 (16), 4422–4433.
Nayler, W.G., Chipperfield, D., Lowe, T.E., 1969. Cardiovasc. Res. 3 (1), 30–36.
Nguyen, N.-T., Wu, Z., 2005. J. Micromech. Microeng. 15 (2), R1–R16.
Oliveira, D.L., Cardoso, V.F., Britto-Júnior, J., Fuguhara, V., Frecentese, F., Sparaco, R., Santagada, V., Caliendo, G., Pupo, A.S., Antunes, E., Nucci, G. de, 2025. Naunyn-Schmiedeberg's. Arch. Pharmacol. 398 (4), 3965–3976.
Pasquier, E., Ciccolini, J., Carre, M., Giacometti, S., Fanciullino, R., Pouchy, C., Montero, M.-P., Serdjebi, C., Kavallaris, M., André, N., 2011. Oncotarget 2 (10), 797–809.
Pereiro, I., Fomitcheva Khartchenko, A., Petrini, L., Kaigala, G.V., 2019. Lab Chip 19 (14), 2296–2314.
Pfeiffer, S.A., Rudisch, B.M., Glaeser, P., Spanka, M., Nitschke, F., Robitzki, A.A., Schneider, C., Nagl, S., Belder, D., 2018. Anal. Bioanal. Chem. 410 (3), 853–862.
Plutschack, M.B., Pieber, B., Gilmore, K., Seeberger, P.H., 2017. Chem. Rev. 117 (18), 11796–11893.
Raby-Buck, S.E., Devlin, J., Gupta, P., Battilocchio, C., Baumann, M., Polyzos, A., Slater, A.G., Browne, D.L., 2025. Nat. Rev. Methods Primers 5 (1).
Santana, H.S., Palma, M.S.A., Lopes, M.G.M., Souza, J., Lima, G.A.S., Taranto, O.P., Silva, J.L., 2020. Ind. Eng. Chem. Res. 59 (9), 3794–3810.
Schmidt, S., Haensch, T., Frank, R., Jahnke, H.-G., Robitzki, A.A., 2021. ACS Appl. Mater. Interfaces 13 (49), 59185–59195.
Tran, V.A., Tran, N.H.T., Bach, L.G., Nguyen, T.D., Nguyen, T.T., Nguyen, T.T., Nguyen, T.A.N., Vo, T.K., Vo, T.-T.T., van Le, T., 2020. J. Chem. 2020, 1–10.
Turgeon, R.T., Bowser, M.T., 2009. Anal. Bioanal. Chem. 394 (1), 187–198.
Wang, X., Liu, J., Wang, P., deMello, A., Feng, L., Zhu, X., Wen, W., Kodzius, R., Gong, X., 2018. Genes 9 (6).
Westphal, H., Schmidt, S., Lama, S., Polack, M., Weise, C., Oestereich, T., Warias, R., Gulder, T., Belder, D., 2024. React. Chem. Eng. 9 (7), 1739–1750.
Westphal, H., Warias, R., Weise, C., Ragno, D., Becker, H., Spanka, M., Massi, A., Gläser, R., Schneider, C., Belder, D., 2022. React. Chem. Eng. 7 (9), 1936–1944.
Zitzmann, F.D., Jahnke, H.-G., Nitschke, F., Beck-Sickinger, A.G., Abel, B., Belder, D., Robitzki, A.A., 2017a. Lab Chip 17 (24), 4294–4302.
Zitzmann, F.D., Jahnke, H.-G., Pfeiffer, S.A., Frank, R., Nitschke, F., Mauritz, L., Abel, B., Belder, D., Robitzki, A.A., 2017b. Anal. Chem. 89 (24), 13550–13558.
Zitzmann, F.D., Schmidt, S., Frank, R., Weigel, W., Meier, M., Jahnke, H.-G., 2024. Biosens. Bioelectron. 250, 116042.
Zitzmann, F.D., Schmidt, S., Naumann, M., Belder, D., Jahnke, H.-G., Robitzki, A.A., 2022. Biosens. Bioelectron. 202, 114010.